

# Vorticity moments in four numerical simulations of the 3D Navier-Stokes equations

**D. Donzis**

<sup>1</sup>Department of Aerospace Engineering, Texas A&M University,  
College Station, Texas, TX 77840, USA

**J. D. Gibbon**

Department of Mathematics, Imperial College London, London SW7 2AZ, UK

**A. Gupta**

Department of Physics, Indian Institute of Science, Bangalore 560 012, India

**R. M. Kerr**

Department of Mathematics, University of Warwick, Coventry CV4 7AL, UK

**R. Pandit**

Department of Physics, Indian Institute of Science, Bangalore 560 012, India  
and  
Jawaharlal Nehru Centre for Advanced Scientific Research, Bangalore, India

**D. Vincenzi**

CNRS, Laboratoire Jean-Alexandre Dieudonné,  
Université de Nice Sophia Antipolis, Nice 06050, France

The issue of intermittency in numerical solutions of the 3D Navier-Stokes equations on a periodic box  $[0, L]^3$  is addressed through four sets of numerical simulations that calculate a new set of variables defined by  $D_m(t) = (\varpi_0^{-1} \Omega_m)^{\alpha_m}$  for  $1 \leq m \leq \infty$  where  $\alpha_m = \frac{2m}{4m-3}$  and  $[\Omega_m(t)]^{2m} = L^{-3} \int_V |\boldsymbol{\omega}|^{2m} dV$  with  $\varpi_0 = \nu L^{-2}$ . All four simulations unexpectedly show that the  $D_m$  are ordered for  $m = 1, \dots, 9$  such that  $D_{m+1} < D_m$ . Moreover, the  $D_m$  squeeze together such that  $D_{m+1}/D_m \nearrow 1$  as  $m$  increases. The first simulation is of very anisotropic decaying turbulence; the second and third are of decaying isotropic turbulence from random initial conditions and forced isotropic turbulence at constant Grashof number respectively; the fourth is of very high Reynolds number forced, stationary, isotropic turbulence at up to resolutions of  $4096^3$ .

## I. INTRODUCTION

### A. Background

Intermittency in both the vorticity and strain fields is a dominant feature of developing and developed turbulence. It has been studied extensively both experimentally (Sreenivasan 1985, Meneveau and Sreenivasan 1991) and numerically (Kerr 1985, Jimenez, Wray, Saffman and Rogallo 1993, Donzis, Yeung and Sreenivasan 2008, Ishihara, Gotoh and Kaneda 2009, Donzis and Yeung 2010, Donzis, Sreenivasan and Yeung 2012, Yeung, Donzis and Sreenivasan 2012). Statistical physicists generally use velocity structure functions to study this phenomenon and have diagnosed the degree of intermittency by how much the velocity structure function exponents  $\zeta_p$  differ from linear when  $p > 3$  (Frisch 1995, Schumacher, Yakhot and Sreenivasan 2007, Boffetta, Mazzino and Vulpiani 2008, Pandit, Perlekar and Ray 2009). The standard way to quantify equal-time, multi-scaling exponents is a challenging numerical task (Arneodo *et al.* 2008, Ray, Mitra and Pandit 2008, Ray, Mitra, Perlekar and Pandit 2011). The multi-scaling approach is even more challenging for the 3D Navier-Stokes equations

$$\partial_t \mathbf{u} + \mathbf{u} \cdot \nabla \mathbf{u} = \nu \Delta \mathbf{u} - \nabla P \quad \text{div } \mathbf{u} = 0 \quad (1)$$

because the velocity field  $\mathbf{u}(\mathbf{x}, t)$  and pressure  $P(\mathbf{x}, t)$  evolve in time, so, in general, time-dependent structure functions must be used to study dynamic multi-scaling (Ray, Mitra and Pandit 2008, Ray, Mitra, Perlekar and Pandit 2011). This paper will introduce an analysis of some new and existing numerical computations that gives new insights into and provides a new method for distinguishing alternative

regimes of behaviour in the vorticity field. To explain the nature of these regimes, let us consider the vorticity field  $\boldsymbol{\omega} = \text{curl } \mathbf{u}$  on a finite periodic domain  $[0, L]^3$  within the setting of the volume integrals which define a set of frequencies

$$\Omega_m(t) = \left( L^{-3} \int_V |\boldsymbol{\omega}|^{2m} dV \right)^{1/2m}, \quad 1 \leq m \leq \infty. \quad (2)$$

Some recent work has centred around a dimensionless re-scaling of the  $\Omega_m$  such that (Gibbon 2010, 2011, 2012a,b)

$$D_m(t) = (\varpi_0^{-1} \Omega_m)^{\alpha_m}, \quad \alpha_m = \frac{2m}{4m-3}, \quad (3)$$

where  $\varpi_0$  is a fixed frequency defined by  $\varpi_0 = \nu L^{-2}$ . The origin of this re-scaling, valid for both the Navier-Stokes and Euler equations, has been explained elsewhere (Gibbon 2011, 2012a,b) where it has been shown that, with additive  $L^2$ -forcing, weak solutions obey the time average up to time  $T$

$$\langle D_m \rangle_{\text{time av.}} \leq c Re^3 + O(T^{-1}). \quad (4)$$

The first in the hierarchy,  $D_1 = \varpi_0^{-2} Z$ , is proportional to the global enstrophy  $Z = \Omega_1^2$  and may be insensitive to deep fine-scale fluctuations. The higher  $D_m$  may be more sensitive so their measurement over a wide range of  $m$  could be a useful diagnostic of intermittency. However, the end of the sequence,  $D_\infty(t)$ , is hard to measure numerically, especially in highly intermittent flows. While Hölder's inequality enforces a natural ordering on the frequencies  $\Omega_m$  such that  $\Omega_m \leq \Omega_{m+1}$  for  $1 \leq m \leq \infty$ , no such natural ordering is enforced on the  $D_m$  because the  $\alpha_m$  decrease with  $m$ . Thus there are two possible regimes:

$$D_{m+1}(t) < D_m(t), \quad (\text{regime I}), \quad D_m(t) \leq D_{m+1}(t), \quad (\text{regime II}). \quad (5)$$

The issues to be addressed in this paper in our four numerical simulations of the 3D Navier-Stokes equations are:

1. Which of these regimes is favoured or is there an oscillation between them? If one regime is favoured, are the  $D_m$  well separated? What is the role of the enstrophy  $D_1$ ?
2. Are these processes  $m$ -dependent?
3. Are they  $Re$ -dependent?
4. Are they dependent upon initial conditions?

## B. Simulations used for tests

An important point with respect to numerical simulations of the scaled higher order moments  $D_m(t)$  is that their ratios might converge better than their actual values. This is consistent with the results reported in Yeung *et al.* (2012) and Donzis *et al.* (2012) where convergence for the ratios of higher-order vorticity and dissipation (strain) moments were obtained, even when the statistics of the individual moments showed no evidence of convergence (Kerr 2012a). This answered a problem first raised in Kerr (1985) where it was noted that in forced simulations at modestly high Reynolds numbers, the averages of the vorticity and strain moments above 6-th order did not converge. The determination of the  $D_m(t)$  in simulations is not difficult whereas, in contrast, traditional numerical tools such as higher-order structure functions require a combination of larger domains and finer resolution than is currently feasible. This paper will calculate and compare the  $D_m(t)$  from four data sets: two where the average kinetic energy  $E = L^{-3} \int_V \frac{1}{2} |\mathbf{u}|^2 dV$  decays in time, and two where  $E$  is held approximately constant by forcing at the low wavenumbers. The first is a unique data set from a computation in which fully-developed turbulence forms from the interaction of two anti-parallel vortices and whose kinetic energy  $E$  decays strongly after the first peak in the normalised enstrophy production  $-S_u$ . Because this calculation has not been fully described before, some introductory discussion is provided at the start of that section (§II). The other three data sets represent more traditional decaying and forced homogeneous, isotropic numerical turbulence. In the decaying calculations in §II and the decaying and forced calculations in §III the

moments have been determined relatively continuously in time which makes a helpful comparison with the results of §I. For the fourth data (4096<sup>3</sup>) set of §IV (Yeung *et al.* 2012, Donzis *et al.* 2012), a similar conclusion is reached by studying the dependence of the average value of  $D_m$  on the Reynolds number.

An advantage of the first data set described in §II is that the predicted convergence properties of ratios of the  $D_m(t)$  can be tested for a calculation with huge fluctuations in the production of enstrophy, and therefore in the higher  $D_m(t)$ . That the calculation eventually exhibits traditional turbulent statistics and spectra is a bonus in justifying its use. However, this new initial condition is very specialized and any trends need to be confirmed using a more traditional decaying homogeneous, isotropic data set, which is the purpose of the second calculation discussed in §III. §III also contains forced simulations of homogeneous and isotropic turbulence at constant Grashof number. Finally, the fourth calculation in §IV provides validation from a forced, massively parallel, pseudo-spectral calculation (4096<sup>3</sup> with  $R_\lambda \approx 1000$ ) calculation to show that these trends are not restricted to low or moderate Reynolds numbers. Assessing the scaling of moments of intermittent quantities such as vorticity, strain rates or velocity gradients has been a critical component of characterizing and understanding intermittency. Of particular interest is how these moments scale with the Reynolds number, which is typically high in applications. At the same time, different orders provide information about fluctuations of different intensities. Low and high-order moments, for example, are associated with weak and strong fluctuations. Thus, the understanding of the scaling of the moments  $D_m$ , especially at high  $m$ , can also shed light on the nature of intermittency and the most extreme events in turbulence.

### C. A summary of results

The simulations described in §II, §III and §IV, and illustrated in Figs. 1, 2 and 5, each observe that a strict ordering of the  $D_m$  occurs, as in regime I; namely  $D_{m+1} < D_m$  (on log-linear plots). To assess the significance of this, we write down the relation  $D_{m+1} < D_m$  in terms of  $\Omega_m$  and use Hölder's inequality  $\Omega_m \leq \Omega_{m+1}$  on the extreme left hand side

$$\varpi_0^{-1} \Omega_m \leq \varpi_0^{-1} \Omega_{m+1} < (\varpi_0^{-1} \Omega_m)^{\alpha_m / \alpha_{m+1}}. \quad (6)$$

As  $m \rightarrow \infty$ ,  $\alpha_m \searrow \alpha_{m+1}$ , and so (6) shows that  $\Omega_{m+1} / \Omega_m \searrow 1$ . Thus, in regime I the  $\Omega_m$  must be squeezed together for high  $m$ . In terms of the  $D_m$  (6) is written as

$$D_m^{\alpha_{m+1} / \alpha_m} \leq D_{m+1} < D_m. \quad (7)$$

While respecting the ordering  $D_{m+1} < D_m$ ,  $D_{m+1}$  is squeezed up close to  $D_m$  as  $m \rightarrow \infty$

$$\lim_{m \rightarrow \infty} \frac{D_{m+1}}{D_m} \nearrow 1. \quad (8)$$

This squeezing phenomenon is observed in all four data sets where the  $D_m$ -curves lie very close for  $m > 3$  as in Figs. 1, 2 and 5. Moreover, the values of  $D_1$  in all four simulations lie far above the rest of the  $D_m$  giving rise to a suggestion, explored in §V, that a depletion of nonlinearity is occurring which could be the cause of Navier-Stokes regularity. The most extreme intermittent events are represented by moments at increasingly large  $m$ . Our results suggest the saturation of these high order moments. This is significant as it constrains the shape of the tails of the PDF of vorticity which has been the focus of intense investigations (Kerr 1985, Jimenez *et al.* 1993, Donzis *et al.* 2008, Ishihara *et al.* 2009, Donzis and Yeung 2010, Yeung *et al.* 2012, Donzis *et al.* 2012). The fourth data set (forced, stationary, isotropic turbulence), the results of which are displayed in §IV, furnishes us with the opportunity to compare these results with other results on intermittency available in the literature. For example, within the multifractal model, Nelkin (1990) found that normalized moments of velocity gradients scale as

$$\langle u_x^p \rangle / \langle u_x^2 \rangle^{p/2} \sim Re_\lambda^{d_p}, \quad (9)$$

where  $d_p$  is obtained from the multifractal spectrum and  $\langle \cdot \rangle$  is the usual notation for the statistical average. Using the well-known result  $\langle u_x^2 \rangle \sim (U_0/L)^2 Re_\lambda^2$  due to the dissipative anomaly, it is readily shown that  $\langle u_x^p \rangle \sim Re_\lambda^{p+d_p}$ . Our interest lies in the limit  $p \rightarrow \infty$  where it can be shown that  $\lim_{p \rightarrow \infty} d_p/p = c$ .

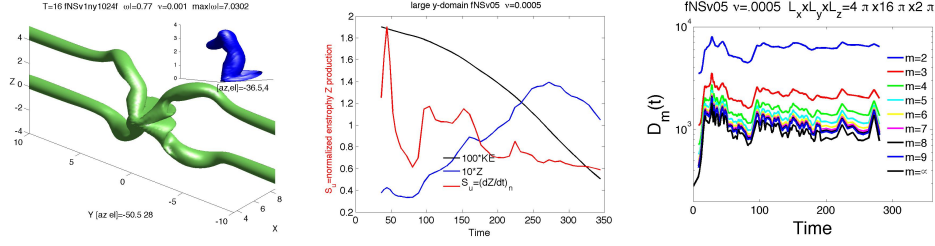


FIG. 1: **First panel:** The initial condition is characterized by long anti-parallel vortices with a localized perturbation for the  $Re = 4000$  reconnection calculation. **Second panel:** Plots of the kinetic energy decay  $E$ , the enstrophy  $Z$  and its production, normalised to be consistent with experimental measurements of the velocity derivative skewness  $-S_u$ .  $Z$  grows until  $t \approx 270$ , while  $E$  is always decaying. **Third panel:** Curves range from  $m = 2$  to  $m = 9$  and include the maximum of vorticity  $D_\infty$ . The normalized enstrophy,  $D_1$ , is far above the log-scale given here, so it is omitted. The  $D_m$  are ordered for all values of  $Re$  and all times.

The constant  $c$  is given by  $c = 3(1 - \mathcal{D}_\infty)/(3 + \mathcal{D}_\infty)$  with  $\mathcal{D}_\infty$  representing the limit  $\lim_{q \rightarrow \infty} \mathcal{D}_q$  of the generalized dimensions  $\mathcal{D}_q$  (Nelkin 1990, Hentschel and Procaccia 1983). Clearly moments of the form  $\langle u_x^p \rangle^{1/p}$  saturate at high  $p$ , consistent with (8). While experimentally it is difficult to measure  $\mathcal{D}_\infty$  reliably, its value appears to be smaller than 1.0 (Meneveau and Sreenivasan 1991). The ratio of successive orders is

$$\langle u_x^{p+1} \rangle^{1/(p+1)} / \langle u_x^p \rangle^{1/p} \sim Re_\lambda^{(1+d_p/p) - (1+d_{p+1}/(p+1))}. \quad (10)$$

The limiting behavior of  $d_p$  shows that  $\lim_{p \rightarrow \infty} [(1 + d_p/p) - (1 + d_{p+1}/(p+1))] = 0$ , and therefore the ratio on the left hand side of (10) tends to a constant independent of  $p$  and  $Re_\lambda$ . This is consistent with the squeezing together of the  $\Omega_m$  and  $D_m$ .

## II. THE FIRST SET OF SIMULATIONS

The new vortex reconnection calculation displayed in this section addresses the following long-standing numerical question: Can an initial condition with only a few vortices generate and sustain fully-developed turbulence through reconnection events in a manner similar to how turbulence forms in aircraft wakes or when anti-parallel quantum vortex lines reconnect numerically (Kerr 2011)? Because this initial condition has not been fully explained before, some of its unique features are now described. The three directions in the flow are: (i) each initial vortex primarily points in the  $\pm y$ -direction; (ii) separation between the vortices lies in the  $z$ -direction; (iii) they propagate in the  $x$ -direction. Due to the anisotropy of the flow, an anisotropic mesh and domain are used with a  $L_x \times L_y \times L_z = 2\pi(2 \times 8 \times 1)$  domain and a  $n_x \times n_y \times n_z = 512 \times 2048 \times 512$  mesh, plus symmetries used in the  $y$  and  $z$  directions. The quantum vortex work in Kerr (2011) has shown that the two most important properties are that their initial perturbations need to be localized far from the periodic boundaries and their initial profile and direction should be balanced so that they are neither internally unstable nor prone to the shedding of waves or vortex sheets. The method grew from addressing calculations identified by Bustamante and Kerr (2008), where a single sign of the initial local vorticity had not been imposed rigorously. To accomplish these goals, the following four changes have been made to the initial condition in Bustamante and Kerr (2008): i) The perturbation is strongly localised near the symmetry plane using the trajectory given in Kerr (2011); ii) The initial vorticity profile uses the solution of a two-dimensional vortex with a smoothed core; iii) The direction of vorticity chosen at grid points follows the path of the nearest point in 3D space on the prescribed trajectory of the central vortex line; iv) The vortices need to be twice as long as in any previous anti-parallel study. Fig. 1 (left) shows the vorticity as the initial instability saturates. By using these choices, regions of negative vorticity and vortex sheets on the  $y = 0$  plane, as described by Bustamante and Kerr (2008), are eliminated.

The ultimate goal is to generate turbulence with a persistent  $-5/3$  energy spectrum and additional turbulent statistics, including the experimental velocity derivative skewness  $S_u = \langle u_x^3 \rangle / \langle u_x^2 \rangle^{3/2}$ , which is equivalent to the numerical normalized enstrophy production. The latest infinite  $Re$ -estimates of  $S_u$  from forced turbulence calculations (Ishihara *et al.* 2009) find  $-S_u \approx 0.68$ , consistent with experimental values of  $-S_u \sim 0.5 - 0.7$ . Early numerical calculations showed that the  $S_u$  tended to overshoot the

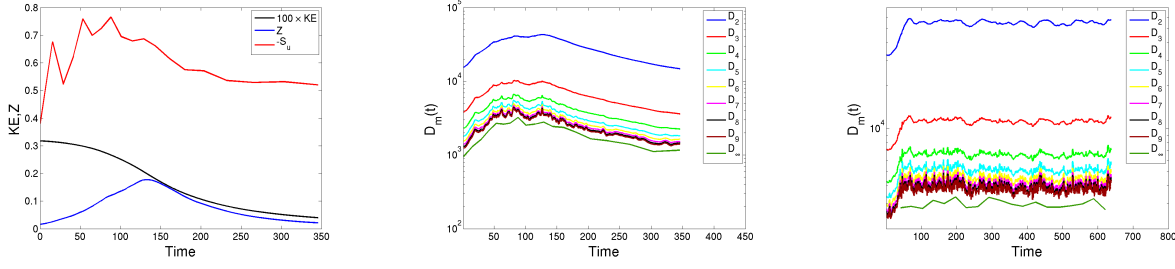


FIG. 2: Plots versus time  $t$  of the total kinetic energy (first panel, black curve), the enstrophy  $Z$  (first panel, blue curve), the normalized enstrophy-production rate  $-S_u$  (first panel, red curve),  $D_m$  for  $2 \leq m \leq 9$  (second panel, blue to brown curves), and  $D_\infty$  (second panel, dark green curve) for our DNS of decaying, 3D Navier-Stokes turbulence; the value of  $D_1$  is very high, so it is omitted. The third panel is of statistically steady forced turbulence at constant Grashof number. The mean values of  $D_m$  in the statistically steady state are as follows:  $\langle D_1 \rangle = 3.1 \times 10^{11}$ ,  $\langle D_2 \rangle = 5.5 \times 10^4$ ,  $\langle D_3 \rangle = 1.1 \times 10^4$ ,  $\langle D_4 \rangle = 6.6 \times 10^3$ ,  $\langle D_5 \rangle = 5.2 \times 10^3$ ,  $\langle D_6 \rangle = 4.5 \times 10^3$ ,  $\langle D_7 \rangle = 4.1 \times 10^3$ ,  $\langle D_8 \rangle = 3.9 \times 10^3$ ,  $\langle D_9 \rangle = 3.7 \times 10^3$ , and  $\langle D_\infty \rangle = 3.0 \times 10^3$ . Zooming in to the right panel makes it clear that  $D_{m+1} < D_m$  for all values of  $m$  considered.

early experimental values of  $-S_u \approx 0.4 - 0.5$  before settling to the expected value (Orszag and Patterson 1972). The second panel of Fig. 1 confirms this trend for the anti-parallel calculation with  $-S_u$  first rising to  $-S_u = 1.9$  at  $t \approx 45$ , then falling abruptly to  $-S_u \approx 0.6$  at  $t \approx 80$ , continuing to fluctuate strongly between 0.6 and 1.2 for  $100 < t < 250$ , and finally decaying to  $-S_u \approx 0.6$ . The full details, plus the relationship between the variations in  $D_m$  in Fig. 1 and the development of swirling, turbulent vortex rings, is the topic of another paper (Kerr 2012b).

In Fig. 1, note that for all times, all of the lower order  $D_m$  ( $m = 1, \dots, 9$ ) bound each higher-order  $D_m$  (on a log-scale) which can be expressed as  $D_{m+1}(t) < D_m(t)$ , thus favouring regime I as in (5). The enstrophy  $D_1$  lies far above all of the other curves and has been omitted. Next note a strong increase in the growth of each of the  $D_m$ , including  $D_\infty$ , up until  $t \approx 16$ . This is the period when this calculation has nearly Euler dynamics, where the effects of viscosity compared to nonlinear growth are minimal. The growth of the  $D_m(t)$  in true Euler dynamics is the topic of another paper (Kerr 2012c).

### III. THE SECOND AND THIRD SET OF SIMULATIONS: DNS RESULTS FOR HOMOGENEOUS, ISOTROPIC TURBULENCE

Data from two direct numerical simulations (DNSs) of homogeneous, isotropic 3D Navier-Stokes turbulence is now presented. Both of these simulations use a pseudospectral method, a 2/3-rule for de-aliasing, and  $512^3$  collocation points on a  $[0, 2\pi]^3$  domain. The first DNS is of decaying turbulence which reaches a Taylor-microscale Reynolds number  $Re_\lambda \simeq 134$  at the main peak of the enstrophy  $Z$  associated with the formation of the inertial sub-range. The Taylor-microscale  $\lambda$  is defined in the usual way in terms of the energy spectrum  $E(k)$ . The initial Fourier components of the velocity  $\tilde{\mathbf{u}}_0(\mathbf{k})$  for the wave-vector  $\mathbf{k} = |\mathbf{k}|$  are generated by applying random phases to the energy spectrum  $E_0(k) = E_0 k^4 \exp\{-2k^2\}$ . The second DNS is a study of statistically steady turbulence which attains  $Re_\lambda \simeq 182$ ; the forcing term  $\mathbf{f}_u(\mathbf{x}, t)$  is specified most simply in terms of  $\tilde{\mathbf{f}}_u(\mathbf{k}, t)$  whose spatial Fourier components are:

$$\tilde{\mathbf{f}}_u(\mathbf{k}, t) = \frac{\mathcal{P}\Theta(k_f - k)}{\sqrt{2E_u(k_f, t)}} \mathbf{u}(\mathbf{k}, t), \quad E_u(k_f, t) = \sum_{k \leq k_f} E_u(\mathbf{k}, t), \quad (11)$$

where  $\Theta$  is the Heaviside function and  $k_f = 2$  is the wave number above which Fourier modes are not forced. This forcing term maintains a constant Grashof number  $Gr = L^3 \mathcal{P} / \nu^2 = 4.9 \times 10^7$ : for a similar forcing term that holds the energy injection fixed see Sahoo, Perlekar and Pandit (2011).

For the decaying DNS, a small inertial subrange forms at  $t = 100$  when the enstrophy  $Z$  reaches its main peak. Assuming  $E_u(k) = K_0(k) \epsilon k^{-5/3}$ , the pre-factor  $K_0(k)$  is roughly 1.5 for about half a decade of wavenumbers. Similar to Fig. 1 (second panel), Fig. 2 (first panel) shows the time-dependence of the kinetic energy  $E$ , enstrophy  $Z$  and its skewness  $-S_u$ . The second and third panels in Fig. 2 show  $D_m$  versus time  $t$  for  $m = 2, \dots, 9$  and  $D_\infty = (\varpi_0^{-1} \|\omega\|_\infty)^{\alpha_\infty}$  with  $\alpha_\infty = \frac{1}{2}$  for both the decaying and forced DNS calculations respectively. The second and third panels also show that  $D_m < D_{m+1}$  and thus demonstrate the generality of Fig. 1 of §II.

$N$	$Re_\lambda$	$k_{max}\eta$	Forcing
256	140	1.4	EP
256	140	1.4	FEK
512	140	2.7	FEK
2048	140	11.2	FEK
512	240	1.4	FEK
2048	240	5.1	FEK
1024	400	1.4	FEK
2048	400	2.8	EP
2048	650	1.4	EP
4096	650	2.7	FEK
4096	1000	1.3	FEK

FIG. 3: Parameters of statistically stationary forced simulations: included are the resolution  $N$ ,  $Re_\lambda$ , the resolution parameter  $k_{max}\eta$  and the forcing type (see text).

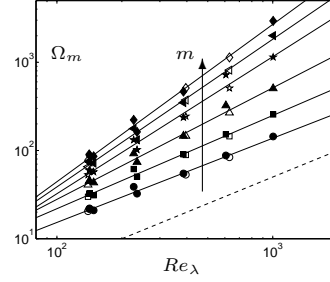


FIG. 4: Scaling of the  $\Omega_m$  as a function of  $Re_\lambda$  for forced stationary isotropic turbulence with resolutions up to  $4096^3$ . Lines are for  $m = 1$  (circles), 2 (squares), 3 (triangles), 4 (stars), 5 (left triangles), 6 (diamonds). Open and closed symbols correspond to EP and FEK forcing respectively. Dashed line is  $\sim Re_\lambda^6$  (see text). Note that for  $Re_\lambda \approx 650$  at  $4096^3$  with FEK forcing, moments up to fourth order (instead of sixth) are available from our database.

#### IV. THE FOURTH SET OF SIMULATIONS: FORCED STATIONARY ISOTROPIC TURBULENCE

The DNS data in this fourth set of simulations were obtained using a massively parallel pseudo-spectral code which achieves excellent performance on  $O(10^5)$  processors. The basic numerical scheme is that of Rogallo (1981). The time stepping is second-order Runge-Kutta and the viscous term is exactly treated via an integrating factor. Aliasing errors are carefully controlled by a combination of truncation and phase shifting techniques. The database includes simulations with resolutions up to  $4096^3$  and Taylor-Reynolds number up to  $Re_\lambda \approx 1000$  (Donzis *et al.* 2012, Yeung *et al.* 2012). In order to maintain a stationary state, turbulence is forced numerically at the large scales. Since our objective is to assess the generality of the ordering of the moments  $D_m$ , here, we show results using the stochastic forcing of Eswaran and Pope (1988) – denoted as EP – as well as a deterministic scheme described in Donzis and Yeung (2010) – denoted as FEK. In essence, this keeps the energy in the lowest wavenumbers fixed. For these two forcing schemes, the wavenumbers affected by forcing are confined to within a sphere  $k < k_F$ , where  $k_F$  is of order 2 or 3. In order to capture intense events, which are the main contributors to high-order moments, resolution issues have to be properly addressed. Motivated by the theoretical work of Yakhot and Sreenivasan (2004), resolution effects have been studied in Donzis (2012), and Yeung *et al.* (2012) with the conclusion that although high-order moments may be under-predicted using the standard resolution criterion – typically in simulations aimed at pushing up the Reynolds number – ratios of high-order moments are weakly affected by resolution issues. Small-scale resolution for a spectral simulation is typically quantified with the parameter  $k_{max}\eta$  where  $k_{max} = \sqrt{2}N/3$  is the highest resolvable wavenumber in a domain of size  $(2\pi)^3$  with  $N^3$  grid points. While the standard resolution is  $k_{max}\eta$  takes values between 1 and 2, results are presented from  $k_{max}\eta \approx 1.5$  to 11, when available, which allows us to assess the effect of insufficient resolution. The Table in Fig. 3 summarizes those parameters of the DNS databased that have been used.

##### A. The $D_m$ -moments in forced stationary isotropic turbulence

Even moments of vorticity  $\Omega_m$  are shown in Fig. 4. As assured by Hölder’s inequality it can be seen that  $\Omega_{m+1} > \Omega_m$  at all Reynolds numbers. The figure also shows the line  $\sim Re_\lambda$  (dashed), which is the result of the dissipative anomaly. This is easily obtained from the kinematic relation  $\langle \epsilon \rangle = \nu \Omega_1^2$  associated with isotropic turbulence and the well-known scaling  $\langle \epsilon \rangle \sim U_0^3/L$ . It can then be shown that  $\Omega_1 \sim (U_0/L)Re^{1/2} \sim (U_0/L)Re_\lambda$ , where the well-known result  $Re_\lambda^2 \sim Re$  has been used. The DNS data in Fig. 4 agree with this scaling. As mentioned above, some resolution effects can be expected especially for high orders. Where data at nominally the same Reynolds number but different resolution is available,

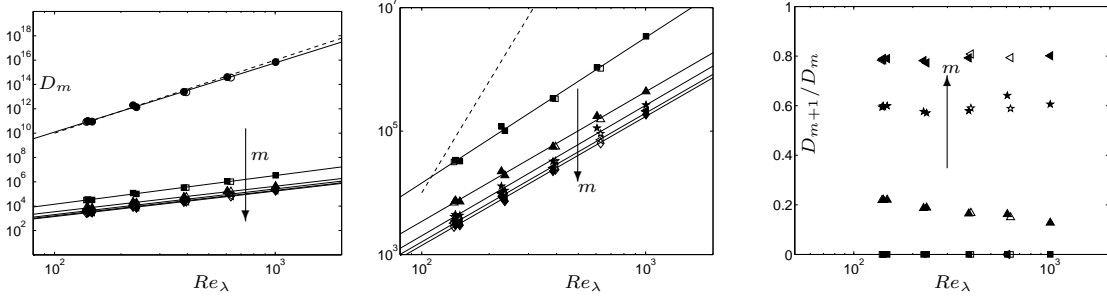


FIG. 5: Scaling of moments of  $D_m$  and ratios as a function of  $Re_\lambda$  for forced stationary isotropic turbulence with resolutions up to  $4096^3$ . **First panel:**  $D_m$  for  $m = 1$  to  $6$ . **Second panel:** Zoom of first panel to highlight the ordering of  $D_m$  for  $m = 2$  to  $6$ . In both parts the dashed lines correspond to  $Re_\lambda^6$ . **Third panel:** Ratio of moments  $D_{m+1}/D_m$  for  $m = 1$  (squares),  $2$  (triangles),  $3$  (stars), and  $4$  (left triangles) as a function of  $Re_\lambda$ .

moments tend to be higher for higher values of  $k_{max}\eta$  (Donzis *et al.* 2008). This is clearer at higher Reynolds number ( $Re_\lambda \approx 650$  where two resolutions are available). Ratios of moments, however, are only weakly affected by resolution, which is also consistent with more recent results (Donzis *et al.* 2012, Yeung *et al.* 2012). In Fig. 5 the moments  $D_m$  are shown as a function of  $Re_\lambda$ . For  $m = 1$ , one can again resort to using the dissipative anomaly with the definition  $D_1 = (\varpi_0^{-1}\Omega_1)^2$ . The result is

$$D_1 = (L^2 \sqrt{\langle \epsilon \rangle} / \nu^{3/2})^2 \sim Re^3 \sim Re_\lambda^6 \quad (12)$$

which is seen in Fig. 5 (first panel). To see further details of higher order moments the second panel in Fig. 5 does not include  $D_1$ . As in §II and §III, the data clearly shows the ordering  $D_{m+1} < D_m$ . The insensitive nature of moments to the type of forcing and the much weaker effect of resolution compared with  $\Omega_m$  in Fig. 4 is also noted. The data also suggest that the ratio between successive moments decreases with  $m$ , which is consistent with the asymptotic behaviour of equation (8). This is more clearly seen in Fig. 5 (third panel) where the ratio of successive moments  $D_{m+1}/D_m$  is plotted for different values of  $m$ . Consistent with an ordering  $D_{m+1} < D_m$ , the ratio is always less than unity. As  $m$  increases, however, this ratio becomes increasingly closer to unity in agreement with Eq. 8. It is also interesting that these ratios appear to be independent of Reynolds numbers which suggest a regime I ordering with clustering of moments at high  $m$  also in the high- $Re_\lambda$  limit. Resolution effects, while weak, can still be seen upon careful examination of the data, especially at high orders. However, for a given simulation, the ordering of regime I is unchanged with resolution.

## V. CONCLUDING REMARKS: THE DEPLETION OF NONLINEARITY

The recent introduction of the  $D_m$ -vorticity-moment-scaling (Gibbon 2011, 2012a,b), motivated by the time average (4), has suggested that they should be calculated through different numerical simulations. All four data sets unexpectedly show that the  $D_m$  obey the ordering of regime I, namely  $D_{m+1} < D_m$ . This leads to the squeezing effect of (8) taking place such that  $\Omega_{m+1}/\Omega_m \searrow 1$  and  $D_{m+1}/D_m \nearrow 1$  as  $m$  increases, which has an effect on the shapes of the PDF-tails, as remarked in §IC. The ordering in the  $D_m$  is strict although for  $m \geq 3, 4$  the plots almost touch and replicate each other in shape as in Figs. 1, 2 and 5 even during intense events. It might be asked whether this is a viscous effect, or a strictly nonlinear effect, or the result of some surprising symbiosis between the two? Using a variation of the anti-parallel initial condition used in §II, new Euler calculations have repeated this observed ordering (Kerr 2012c), which implicates the nonlinear terms as the source. However, there is no evidence from Navier-Stokes analysis that such an ordering should hold, although no results exist that suggest it cannot. It is, of course, possible that a cross-over could occur between regimes I and II at Reynolds numbers higher than have been achieved in this work.

Significantly  $D_1$  sits well above the other  $D_m$  and does not appear to converge with them during the most intense periods: in Figs. 1, 2 and 5  $D_m$  lies on a log-scale with  $D_1$  omitted. We are therefore justified in writing

$$\ln D_m \lesssim a_m \ln D_1 \quad \Rightarrow \quad D_m \lesssim D_1^{a_m}. \quad (13)$$

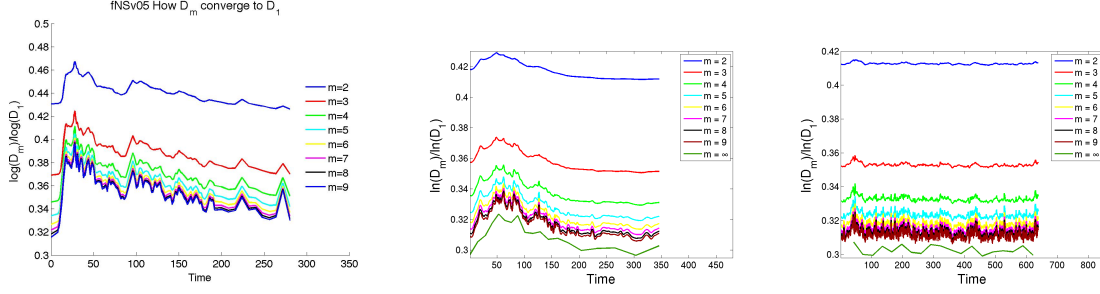


FIG. 6: Plots of  $a_m$  for the three simulations in respectively §II and §III in which  $a_m < \frac{1}{2}$ .

Plots of  $a_m$  for the first and second pair of simulations are shown in Fig. 6. Assuming a solution exists, the  $D_m$  have been shown to obey (see Gibbon 2012a)

$$\dot{D}_m \leq D_m^3 \left\{ -\varpi_{1,m} \left( \frac{D_{m+1}}{D_m} \right)^{\frac{2}{3}m(4m+1)} + \varpi_{2,m} \right\}, \quad (14)$$

where the  $c_{n,m}$  within  $\varpi_{1,m} = \varpi_0 \alpha_m c_{1,m}^{-1}$  and  $\varpi_{2,m} = \varpi_0 \alpha_m c_{2,m}$  are algebraically increasing with  $m$ . By dropping the negative term on the right hand side of (14), and replacing the  $D_m^3$ -term with  $D_m D_1^{2a_m}$  justified by (13), a time integration produces

$$D_m(t) \leq c_m \exp \int_0^t D_1^{2a_m} d\tau \leq c_m \exp \left\{ t^{1-2a_m} \left( \int_0^t D_1 d\tau \right)^{2a_m} \right\} \quad 2a_m \leq 1. \quad (15)$$

Fig. 6 shows that while there is a weak dependence of  $a_m$  on both  $m$  and  $t$ , it nevertheless satisfies  $2a_m < 1$  in all cases. Because Leray's energy inequality insists that  $\int_0^t D_1 d\tau < \infty$  it is clear that the right hand side of (15) is finite: *any* finite  $D_m$  is sufficient for Navier-Stokes regularity. This regularization can thus be traced to the *depletion of nonlinearity* in (13) in regime I. Although regime II has not been observed, (14) shows that it is associated with time-decay of the  $D_m$ . Specifically, if  $D_{m+1}/D_m \geq [c_{1,m} c_{2,m}]^{3/2m(4m+1)}$  then  $\dot{D}_m < 0$  where  $[c_{1,m} c_{2,m}]^{3/2m(4m+1)} \searrow 1$  for large  $m$ .

**Acknowledgements:** DD acknowledges the computing resources provided by the NSF-supported XSEDE and DOE INCITE programs under whose auspices some of these calculations were performed. RP and DV are members of the International Collaboration for Turbulence Research (ICTR). They acknowledge support from the “Indo-French Center for Applied Mathematics”, UMI IFCAM – Bangalore and, with RMK, the EU COST Action program MP0806 “Particles in Turbulence”. AG and RP thank DST, CSIR and UGC (India) and the SERC (IISC) for computational resources. JDG and RMK thank the Isaac Newton Institute, Cambridge, on whose programme *Topological dynamics in the Physical and Biological sciences (2012)* part of this work was carried out.

- 
- [1] Arneodo, A., Benzi, R., Berg, J., Biferale, L., Bodenschatz, E., Busse, A., Calzavarini, E., Castaing, B., Cencini, M., Chevillard, L., Fisher, R. T., Grauer, R., Homann, H., Lamb, D., Lanotte, A. S., Leveque, E., Luethi, B., Mann, J., Mordant, N., Mueller, W.-C., Ott, S., Ouellette, N. T., Pinton, J.-F., Pope, S. B. Roux, S. G. Toschi, F. Xu, H. and Yeung, P.K. 2008 Universal Intermittent Properties of Particle Trajectories in Highly Turbulent Flows. *Phys. Rev. Lett.* **100**, 254504.
  - [2] Betchov, R. 1956 An inequality concerning the production of vorticity in isotropic turbulence. *J. Fluid Mech.* **1**, 497–504.
  - [3] Boffetta, G., Mazzino, A. and Vulpiani, A. 2008 Twenty-five years of multifractals in fully developed turbulence: a tribute to Giovanni Paladin. *J. Phys. A: Math. Theor.* **41**, 363001.
  - [4] Bustamante, M. D. and Kerr, R. M. 2008 3D Euler about a 2D symmetry plane. *Physica D* **237**, 1912–1920.
  - [5] Donzis, D., Yeung, P. K. and Sreenivasan, K. 2008 Dissipation and enstrophy in isotropic turbulence: scaling and resolution effects in direct numerical simulations. *Phys. Fluids* **20**, 045108.
  - [6] Donzis, D. and Yeung, P. K. 2010 Resolution effects and scaling in numerical simulations of passive scalar mixing in turbulence. *Physica D* **239**, 1278–1287.
  - [7] Donzis, D., Sreenivasan, K. and Yeung, P. K. 2012 Some results on the Reynolds number scaling of pressure statistics in isotropic turbulence. *Physica D* **241**, 164–168.
  - [8] Eswaran, V. and Pope, S. B. 1988 An examination of forcing in direct numerical simulations of turbulence. *Comput. Fluids* **16**, 257–278.



- [9] Frisch, U. 1995 *Turbulence: the legacy of A. N. Kolmogorov*, Cambridge University Press, Cambridge.
- [10] Gibbon, J. D. 2010 Regularity and singularity in solutions of the three-dimensional Navier-Stokes equations *Proc. Royal Soc A* **466**, 2587–2604.
- [11] Gibbon, J. D. 20011 A hierarchy of length scales for weak solutions of the three-dimensional Navier-Stokes equations. *Comm Math. Sci.* **10**, 131–136.
- [12] Gibbon, J. D. 2012a Conditional regularity of solutions of the three dimensional Navier-Stokes equations and implications for intermittency. *J. Math. Phys.* **53**, 115608.
- [13] Gibbon, J. D. 2012b Dynamics of scaled vorticity norms for the three-dimensional Navier-Stokes and Euler equations. arXiv:1212.0684. To appear in *Procedia IUTAM: Proceedings of IUTAM Symposium Topological Fluid Dynamics II* Cambridge.
- [14] Hentschel, H. G. E. Procaccia, I. 1983 The infinite number of generalized dimensions of fractals and strange attractors. *Physica D* **8**, 435–444.
- [15] Holm, D. D. and R. M. Kerr, R. M. 2007 Helicity in the formation of turbulence. *Phys. Fluids* **19**, 025101.
- [16] Ishihara, T., Gotoh T., and Kaneda, Y. 2009 Study of high-Reynolds number isotropic turbulence by direct numerical simulation. *Annu. Rev. Fluid Mech.* **41**, 16–180.
- [17] Jimenez, J., Wray, A., Saffman, P. G. and Rogallo, R. S. 1993 The structure of intense vorticity in isotropic turbulence. *J. Fluid Mech.* **255**, 65–90.
- [18] Kerr, R. M. 1985 Higher-order derivative correlations and the alignment of small-scale structures in isotropic numerical turbulence. *J. Fluid Mech.* **153**, 31–58.
- [19] Kerr, R. M. 1993 Evidence for a singularity of the three-dimensional incompressible Euler equations. *Phys. Fluids A* **5**, 1725–1746.
- [20] Kerr, R. M. 2011 Vortex stretching as a mechanism for quantum kinetic energy decay. *Phys. Rev. Lett.* **106**, 224501.
- [21] Kerr, R. M. 2012a Dissipation and enstrophy statistics in turbulence: Are the simulations and mathematics converging? *J. Fluid Mech.* **700**, 1–4.
- [22] Kerr, R. M. 2012b Incompressible hydrodynamic turbulence from a chain reaction of vortex reconnection events. arXiv:1212:3829v1 submitted to *Phys. Fluids* as Swirling, turbulent vortex rings forming from a chain reaction of reconnection events.
- [23] Kerr, R. M. 2012c Bounds on a singular attractor in Euler using vorticity moments, <http://arxiv.org/abs/1212.1106>, to appear in *Procedia IUTAM, Proceedings of IUTAM Symposium Topological Fluid Dynamics II* Cambridge.
- [24] Meneveau, C. and Sreenivasan, K. R. 1991 The multifractal nature of turbulent energy dissipation. *J. Fluid Mech.* **224**, 429–484.
- [25] Nelkin, M. 1990 Multifractal scaling of velocity derivatives in turbulence. *Phys. Rev. A* **42**, 7226–7229.
- [26] Orszag, S. A. and Patterson, G. S. 1972 Numerical simulation of three-dimensional homogeneous isotropic turbulence. *Phys. Rev. Lett.* **28**, 76–79.
- [27] Pandit, R., Perlekar, P. and Ray, S. S. 2009 Statistical properties of turbulence: An overview, *Pramana – Journal of Physics* **73**, 157–191.
- [28] Ray, S. S., Mitra, D. and Pandit, R. 2008 The universality of dynamic multiscaling in homogeneous, isotropic Navier-Stokes and passive-scalar turbulence. *New J. Phys.* **10**, 033003.
- [29] Ray, S. S., Mitra, D., Perlekar, P. and Pandit, R. 2011 Dynamic Multiscaling in Two-Dimensional Fluid Turbulence. *Phys. Rev. Lett.* **107**, 184503.
- [30] Rogallo, R. S. 1981 Numerical experiments in homogeneous turbulence. *Tech. Rep.* 81835. NASA Tech. Mem.
- [31] Sahoo, G., Perlekar, P. and Pandit, R. 2011 Systematics of the magnetic-Prandtl-number dependence of homogeneous, isotropic magnetohydrodynamic turbulence. *New J. Phys.* **13**, 013036.
- [32] Schumacher, J., Sreenivasan, K. R. and Yakhov, V. 2007 Asymptotic exponents from low-Reynolds-number flows. *New J. Phys.* **9**, 89–107.
- [33] Sreenivasan, K. R. 1985 On the fine-scale intermittency of turbulence. *J. Fluid Mech.* **151**, 81–103.
- [34] Yakhov, V. and Sreenivasan, K. R. 2004 Towards a dynamical theory of multifractals in turbulence. *Physica A* **343**, 147–155.
- [35] Yeung, P. K., Donzis, D. and Sreenivasan, K. R. 2012 Dissipation, enstrophy and pressure statistics in turbulence simulations at high Reynolds numbers. *J. Fluid Mech.* **700**, 5–15.